Nobeyama/HXT Observations of Impulsive Flares

Masanori Nishio
Department of Physics, Kagoshima Univ., Kagoshima 890-0065 Japan
E-mail(FI): nishio@sci.kagoshima-u.ac.jp
Takeo Kosugi
The Institute of Space and Astronautical Science, Sagamihara, Japan
Kentaro Yaji
Kawabe Cosmic Park, Wakayama, Japan
and
Hiroshi Nakajima
Nobeyama Radio Observatory, Nagano, Japan

Abstract

The results of an analysis of 25 impulsive solar flares, observed simultaneously with the Nobeyama Radioheliograph and the *Yohkoh* satellite, are presented. From the relative locations of microwave, hard X-ray, and soft X-ray sources, we have found that, for half out of the 25 analyzed events, at least two loops are involved. Typical sizes of the two loops are different from each other; one is typically $\leq 20''$ and the other $30''$–$80''$. These observations suggest that in the majority of impulsive flare events two loops interact with each other, releasing magnetic energy and producing energetic electrons.

We have analyzed 2 out of the 25 events in detail and find that a triple source structure corresponding to footpoints of the short and long loops are related by a single event. An analysis of HXT flux spectra and time profiles of these footpoint sources suggests that in these events trapping and diffusion of the high energy electrons in the loops play dominant rolls.

Key words: Solar Flares — Radio — Hard X-ray — Coronal Magnetic Filed

1. Introduction

A comparison of the relative location of microwave and hard X-ray (HXR) solar burst sources, especially impulsive solar burst sources, is important for clarifying whether the particle acceleration site is, in fact, the same for both types of emission and, further, to investigate what magnetic configuration is responsible for the flare energy release. Many authors made microwave and HXR imaging observations and discussed the relative locations of the two types of burst sources (e.g., Hoyng et al. 1983; Kawabata et al. 1982; Takakura et al. 1983, 1994; Kundu 1984; Kundu et al. 1995; Nakajima 1989; Gopalswamy et al. 1995; Wang et al. 1995, 1996). Recently, Nishio et al. (1997, 1998) systematically studied the microwave and HXR images for fourteen impulsive solar flares simultaneously observed in microwaves and HXRs. They showed that both microwaves and HXRs from the flares are mostly emitted from single or double sources. However, the locations of the two types of sources do not necessarily coincide to each other. HXR sources are compact and are located at footpoints of the flaring loops, while the microwave sources show elongated loop-like structures in many cases and are cospatial with soft X-ray (SXR) flaring loops. Even in cases of compact microwave sources, circular polarization images show bipolar source structures in the sources. They suggested that in the majority of impulsive solar flares two loops interact with each other, releasing magnetic energy and producing energetic electrons. The observations are consistent with the emerging flux model of flares (e.g., Heyvaerts et al. 1977). Hanaoka (1996, 1997) also suggested interacting flare loop configurations during flares based on the observations in microwaves and X-rays. He showed that flux emergence was associated with most of the events analyzed.

In this paper, we present results of an analysis for a systematically selected data set of solar impulsive flares (25 events) observed simultaneously with microwave and HXR instruments during solar cycle 22, and discuss the magnetic field configuration during this type of flare. In 2 out of the 25 events, we have analyzed the evolution of the flare's source structure and the HXR flux spectra of individual flare sources in detail.

Table 1.. Summary of observed parameters for 25 events

DATE	TIME (UT)	GOES Class	17GHz Flux[1]	HXT[2] L	M1	M2	H	γ	Source Struc.[3] 17GHz	HXR	Location[4] Helio.(NOAA)	Type[5]
Jun. 25, 1992	03:34:14	C1.8	42	18	22	14	7	2.7	double	single	N16W61(7205)	b-1
Jul. 15, 1992	02:00:05	C4.2	1.6	17	9	2	–	5.6	double	double	S10W44(7220)	a
Aug. 17, 1992	23:58:48	C4.3	131	28	29	10	2	4.7	double	triple	N15W00(7260)	c-2
Aug. 20, 1992	03:51:28	C4.5	63	15	8	3	–	4.5	double	double	N14W23(7260)	b-2
Sep. 6, 1992	01:58:22	M1.0	4	26	17	6	1	4.9	double	triple	S15W33(7270)	c-2
Sep. 11, 1992	02:59:51	M1.0	70	38	23	14	5	3.3	single	double	N11E38(7276)	a?
Sep. 11, 1992	06:04:51	M1.4	410	69	92	71	43	2.5	single	double	N09E31(7276)	c-1?
Oct. 27, 1993	01:45:27	M1.1	114	97	58	25	7	4.2	double	double	S31W20(7321)	c-1?
Oct. 29, 1992	06:32:05	C2.1	120	22	15	5	1	4.8	quad.	triple	S29W47(7321)	c-2
Nov. 5, 1992	06:19:24	M2.0	12	43	34	19	8	3.3	single	single	S16W86(7323)	—
Nov. 22, 1992	23:07:51	M1.6	2.5	47	29	13	5	4.0	double	double	N08E70(7348)	b-2
Dec. 15, 1992	01:11:36	C6.9	18	37	27	11	4	4.4	double	double	S22W42(7360)	c-1
Dec. 16, 1992	03:16:35	C4.6	11	14	11	5	–	4.8	double	double	S21W57(7360)	c-1
Feb. 6, 1993	05:25:59	C5.6	91	38	21	11	5	3.2	double	single	S07E68(7420)	b-1
Apr. 6, 1993	23:44:52	M1.5	82	52	26	10	4	4.7	double	double	S02E04(7469)	b-2
Apr. 10, 1993	23:33:22	C9.1	50	36	36	27	17	2.7	double	single	S05W53(7469)	b-1
Apr. 11, 1993	06:13:38	C8.9	16	29	24	9	3	3.3	double	triple	S04W61(7470)	—
May 28, 1993	02:02:43	C9.1	49	32	24	11	4	4.0	double	double	N19E50(7515)	b-2
May 30, 1993	06:48:57	C2.8	10	15	12	5	–	3.4	triple	triple	N21E14(7515)	—
Jun. 7, 1993	05:42:48	C4.1	50	13	14	8	3	3.4	double	single	S01W29(7518)	b-1
Nov. 30, 1993	06:03:33	C9.2	245	55	68	53	33	2.5	triple	com.	S19W78(7534)	—
Jan. 6, 1994	04:05:30	C4.9	48	19	22	17	10	2.6	double	triple	N09W30(7646)	c-1
Jan. 18, 1994	04:20:47	C2.8	11	16	12	5	–	4.1	single	double	N08E56(7654)	c-2
Jan. 26, 1994	05:40:08	C1.4	420	46	56	47	28	2.4	single	triple	N08W56(7654)	c-2
Apr. 22, 1994	00:19:43	C5.2	13	15	13	9	3	3.1	double	single	N12E11(7705)	b-1

1) In units of sfu.
2) In units of counts s^{-1} $subcollimator^{-1}$, background subtracted.
HXR spectral index, γ, is derived from the ratio of photon count rates between M1- and M2-bands.
3) quad.= quadruple sources, comp.= complex source structure.
4) Heliocentric flare position obtained from microwave images.
5) Types of relative location of the microwave, HXR, and SXR sources, corresponding to the schematic drawings by Nishio et al. (1997, in Figure 2).

2. OBSERVATIONS AND DATA SELECTION

The images used are those simultaneously observed with the Nobeyama Radioheliograph (Nakajima et al. 1994; Nishio et al. 1994) and the *Yohkoh* Hard X-ray Telescope (HXT; Kosugi et al. 1991). The observation frequency of the radioheliograph is 17 GHz, where nonthermal electrons dominating the burst emission have energy $\geq$ 100 keV. The HXT makes two-dimensional solar images in four energy bands: L (13.9–22.7 keV), M1 (22.7–32.7 keV), M2 (32.7–52.7 keV), and H (52.7–92.8 keV). We have also used soft X-ray images taken with the *Yohkoh* Soft X-ray Telescope (SXT; Tsuneta et al. 1991) to identify the loop connectivity of burst sources. From late June 1992, when the Nobeyama Radioheliograph began routine operation, until the end of 1994, 140 flares were simultaneously observed with the radioheliograph and the HXT, of which 49 flares have enough photon counts ($\geq$ 10 counts s^{-1}subcollimator^{-1}) to synthesize HXR images in the HXT M1-band.

The HXR bursts are usually ascribed to the nonthermal electrons, with some exceptions. Both thermal and nonthermal electrons generally contribute to microwave burst emission. As different mechanisms are required to produce the thermal and nonthermal electrons, different loop configurations may be involved in the nonthermal- and thermal-electron-dominant events. In this paper, we have focused to the magnetic field configuration related with the behavior of energetic electrons. Thus, we adopted the following criteria for event selection; (1) time profiles in microwaves and HXRs show a single spike or multiple spikes, with each spike being of $\approx$ 10 s duration, (2) Peak times of spikes in microwaves and HXRs coincide to within a few seconds, and (3) HXR spectra of these spikes have quite hard spectra of less than 5. With these criteria, we selected a total of 25 events, in which 14 events analyzed in a previous paper by Nishio et al. (1997) are included. Recently, the image quality of the HXT is drastically

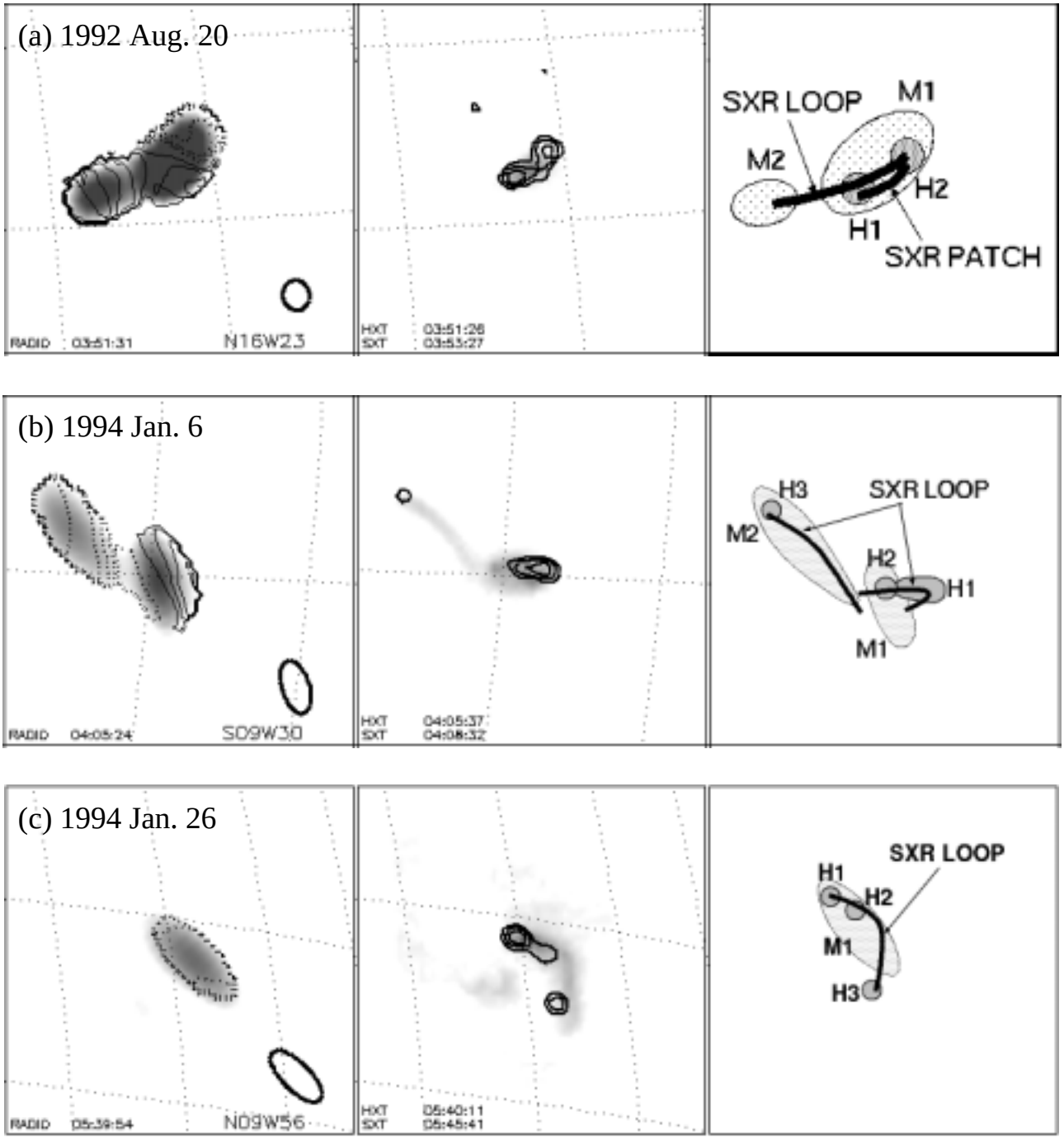

Fig. 1.. Coaligned 17-GHz images (left panels), HXT M1-band images (contours in middle panels), and SXT Be-filter images (gray scale in middle panels) for the 1992 Aug. 20, 1994 Jan. 06 and 1994 Jan. 26 events. The 17-GHz images are shown in brightness temperature in gray scale, and in degree of circular polarization with contour levels of 5, 10, 20, 40, 60, and 80%. Solid and dotted lines correspond to right- and left-circular polarizations, respectively. The gray scales correspond to a range of $0.04\sim0.4 \times 10^6$ K for (a), $0.04\sim1.0 \times 10^6$ K for (b), and $0.04\sim5.0 \times 10^6$ K for (c). A circle of thick solid line shown at bottom-right of each image is the FWHM beam width. HXR contours are drawn at 50%, 25%, and 12.5% levels of the peak intensity. The rightmost panels are cartoons representing the spatial relationships between the microwave, HXR, and SXR sources. The microwave sources are shown by light gray patches (M1, M2), while the HXR sources by dark gray patches (H1, H2, H3). The SXR sources are drawn by thin black lines. The frame size is $2'.6 \times 2'.6$. The top of each frame corresponds to north, and right to west in solar coordinates.

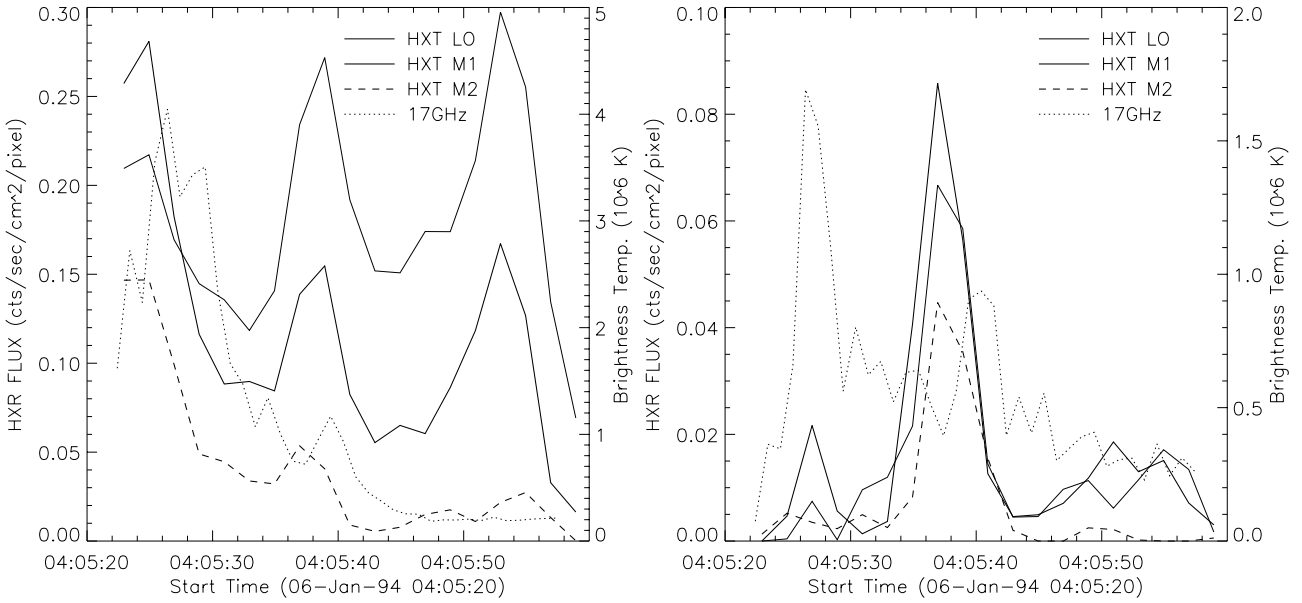

Fig. 2.. HXT M1-band images of the 1994 Jan. 6 event. (a), (b), (c) and (d) correspond to the images at first, a valley between the first and second spikes, the second spike and the third peak, respectively.

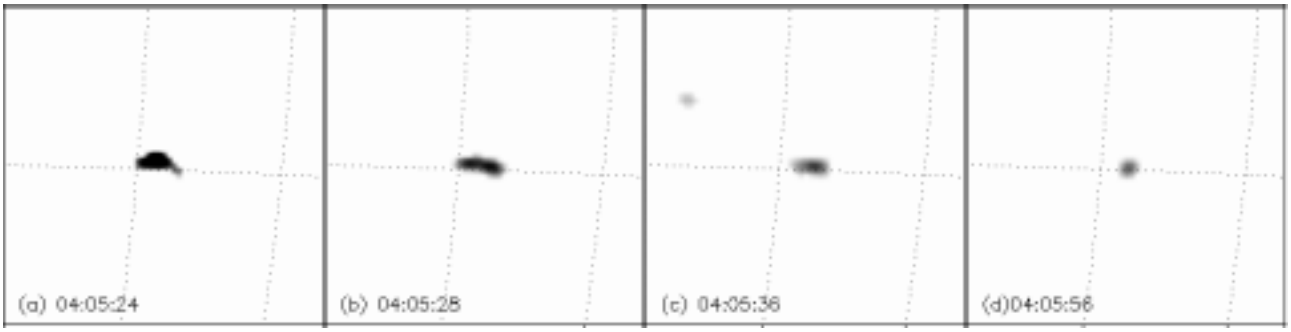

Fig. 3.. Light curves of (a) the double sources and (b) the remote source for the 1994 Jan. 6 event. The HXR flux and microwave brightness temperature of the double sources are given by the average over the region including the two sources.

improved after detailed analysis of critical parameters relating with the imaging performance (Sato 1997). We have re-analyzed the previously presented 14 events in addition to the analysis of 11 new events. Characteristics of these selected 25 events – the peak flux density at 17 GHz, the photon count rates in the four HXT energy bands, and HXR photon spectral indices, γ – are summarized in Table 1.. Times are those of the highest peaks in the HXT M2-band, and the flux density and photon count rates are given for these peaks. The photon spectral indices are derived from the ratio between photon count rates of HXT M1- and M2-bands. Source structures seen in microwave and HXR images and heliocentric coordinates of the brightest microwave sources are also shown in Table 1..

3. RELATIVE LOCATIONS OF MICROWAVE, HARD X-RAY, AND SOFT-XRAY SOURCES

In figure 1., we show coaligned microwave, HXR and SXR images of 3 (the 1992 Aug. 20, 1994 Jan. 6 and 1994 Jan. 26 events) out of the 25 events. The leftmost panels show 17 GHz images; the gray scales show the microwave brightness temperature and the contours indicate the degree of polarization. Contours and gray scales in the middle panels represent HXR and SXR images, respectively. The SXR images are those taken with the Be 119-μm filter whose images show the spatial distribution of relatively hot ($\geq$ 6.5 MK) plasma. The rightmost panels are cartoons

Table 2.. HXR flux and spectra of the double and remote sources.

1994 Jan. 6 event

	TIME	HXR Flux[1]				Flux Ratio		
	(UT)	L	M1	M2	H	L/M1	M1/M2	M2/H
Double Source	04:05:24	0.21	0.28	0.15	—	0.8	1.9	—
	04:05:38	0.27	0.15	0.041	—	1.8	3.8	—
	04:05:52	0.30	0.17	0.022	—	1.8	7.7	—
Remote Source	04:05:26	$(0.007)^2$	0.022	$(0.004)^2$	—	$(0.3)^3$	$(6.2)^3$	—
	04:05:36	0.067	0.086	0.045	—	0.8	1.9	—
	04:05:50	$(0.006)^2$	0.019	—	—	0.3	—	—

1994 Jan. 26 event

	TIME	HXR Flux[1]				Flux Ratio		
	(UT)	L	M1	M2	H	L/M1	M1/M2	M2/H
Double Source	05:39:59	0.48	0.65	0.44	0.19	0.75	1.5	2.3
	05:40:07	0.78	1.1	0.70	0.22	0.72	1.5	3.2
	05:40:11	0.57	0.72	0.41	0.14	0.79	1.8	3.0
Remote Source	05:40:07	0.35	0.18	0.29	0.062	2.0	0.60	4.8
	05:40:11	0.23	0.46	0.22	0.028	0.50	2.1	1.1

[1] In units of counts cm^{-2} s^{-1} $pixel^{-1}$. The flux of the double sources is given by the average over the region including these two sources.
[2] Under the limit of the dynamic range of HXT imaging capability.
[3] Derived by the values under the limit of the dynamic range of HXT imaging capability.

representing the spatial relationships between the microwave, HXR, and SXR sources. The accuracy of coalignment among the microwave, HXR, and SXR images is better than 5″. In the 1992 Aug. 20 and 1994 Jan. 6 events, the microwave images show double sources, one of which (the brighter one) is cospatial with a HXR close double source. In the microwave polarization images, the brighter source shows bipolar structure. In the 1994 Jan. 6 event, another compact HXR source is seen, which is cospatial with the remote edge of the weaker (less bright) microwave source remote from the brighter source. In the SXR image taken ≈ 3 min after the onset of the flare, a patch-like structure cospatial with the HXR double (and brighter microwave) sources and a loop-like structure connecting the HXR double sources and the HXR remote source are clearly seen. The HXR triple source structure, similar with the 1994 Jan. 6 event, is also seen in the 1994 Jan. 26 event. In microwave images, an elongated single source is seen, which is cospatial with the HXR close double. In all the events mentioned above, strong circular polarization is observed over entire microwave structure.

From an analysis of the relative locations of microwave, HXR and SXR sources in 25 impulsive events, most of the events can be classified into one of five types given by Nishio et al. (1997); (a) cospatial microwave/HXR double sources, (b1) double microwave sources with a single HXR source at one side, (b2) double microwave sources with double HXR sources at one side, (c1) double HXR sources with an elongated microwave sources, or (c2) triple HXR sources with an elongated microwave source. In twelve events, of types (b2), (c1) and (c2), the coaligned microwave and HXR images clearly show that three footpoint sources of HXR and/or microwave emission are involved in a single event. Two of these sources, usually seen in HXRs, are in close proximity, with a separation of 10″–20″. The third source, which is seen both in microwaves and HXRs in five events and only in microwaves in the remaining seven events, is located 30″–80″ from the HXR close double. These results is consistent with those given in the previous paper (Nishio et al. 1997).

4. EVOLUTION OF THE FLARE SOURCES

We now investigate the spatial and temporal evolution of the HXR and microwave sources in more detail for two events (the 1994 Jan. 6 and 1994 Jan. 26. events). These events are cases in which multiple flare loops are clearly observed.

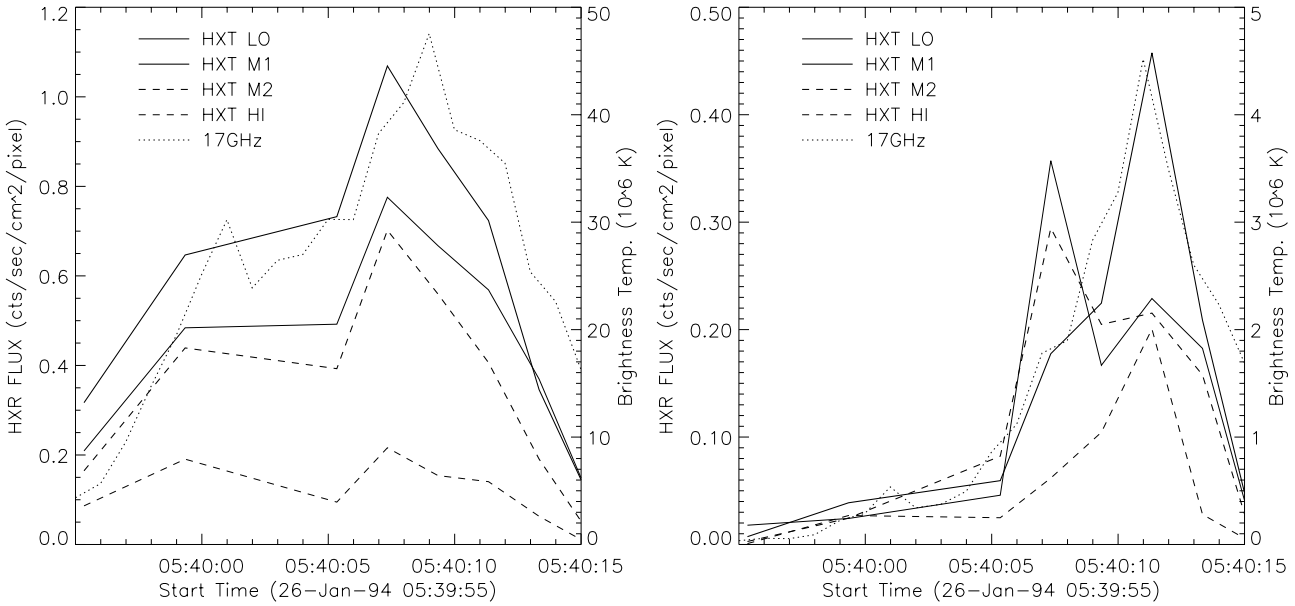

Fig. 4.. Light curves of (a) the double sources and (b) the remote source for the 1994 Jan. 26 event. The HXR flux and microwave brightness temperature of the double source are given by the average over the region including the two sources.

4.1. 1994 Jan. 6 Event

This event occurred in NOAA 7646, which was located at N09W30 in heliocentric coordinates. GOES soft X-ray observations reveal a C4.9-class flare, which peaked at 04:07 UT and had a duration of ≈ 6 min. In HXRs, the burst begins at 04:05:20 UT and its duration is ≈ 1 min, during which three spikes, each of ≈ 5 s duration, are seen. In microwaves, only the first two out of the three HXR spikes are discernible, and the 17-GHz flux gradually decays after the second spike. The HXR spectral indices derived from the photon count rates of M1- and M2-bands are $\gamma = 2.6$, 3.2, and 4.6 during the first, second and third spikes, respectively.

In this event, the spatial relationship between microwave, HXR, and SXR sources changes considerably from spike to spike. As shown in figure 1. (b), the HXR emitting region consists of close-double sources and a compact remote source. The separation between the double sources is $\approx 10''$ in the east-west direction. The location of the HXR maximum in the double source structure is different for these three spikes. Figure 2. shows images at the first spike, a valley between the first and second spikes, the second spike, and the third spikes, respectively. A close-double source is clearly seen at the valley between the first and second spikes (figure 2. (b)). During the first spike, the east source or midway of the two sources is brightest, while during the second spike the west source is brighter than the other. During the third spike, a compact single-source structure is seen, which corresponds to the western component of the HXR double. The third source, that is the compact remote source, is clearly seen during the second spike (figure 2. (c)), while it is faint during the first and third spikes. In a SXR image obtained during the time of the third spike, a compact SXR source cospatial with the HXR remote source appears, which coincides with a footpoint of a long loop seen in a SXR image taken few minutes after the onset of the flare.

The light curves of the double sources and the remote source are shown in figure 3. for the HXT L, M1 and M2-bands. The flux of the close HXR double sources is given by the average over the region including these two sources. Microwave brightness variations in corresponding two regions are also plotted in figure 3.. In this figure, we can find that (1) both the double and remote sources show an impulsive enhancement during the first, second and third spikes, respectively, (2) for the double source the HXR flux spectrum changes hard to soft with time, (3) the HXR spectrum of the remote source is harder than that of the double sources, especially during the second spike, (4) the peak times of the double source and the remote source do not necessarily coincide to each other; during the first spike the HXR peak of the double source precedes the remote source by ≈ 2 s, while during the second spike the HXR peak of the double source is delayed ≈ 2 s to that of the remote source, and (5) the microwave emitting region cospatial with the HXR remote source shows two prominent spikes with the duration of ≈ 3 s; in the first spike its peak time is coincident with that of the HXR remote source, while in the second spike the peak is delayed

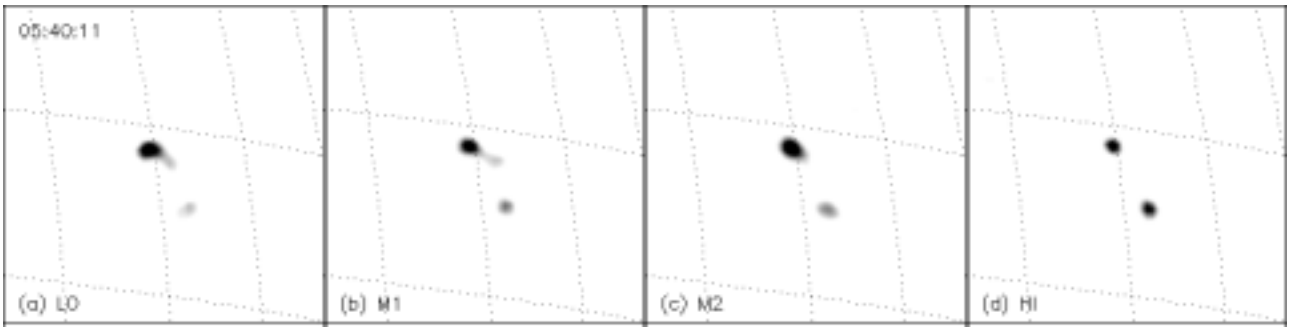

Fig. 5.. HXT L, M1, M2 and Hi-band images of the 1994 Jan. 26 event. These images are taken at the second spike.

$\approx$ 4 s relative to that of the HXR remote source.

4.2. 1994 Jan. 26 Event

This event occurred in NOAA 7654, which was located at N08W56 in heliocentric coordinates. GOES soft X-ray observations reveal a C1.4-class flare, which showed an impulsive intensity enhancement with a duration of $\sim$ 5 min, peaking at 05:41UT. In HXRs, the burst begins at 05:39:59UT and its duration is about 30 s. Two spikes, which peaks are at 05:40:00UT and 05:40:07UT, are evident. The HXR spectral index, derived from the photon count rates of M1- and M2-bands, is $\gamma = 2.4$ for both spikes.

During the second spike, a triple-source structure, i.e., a close-double source and a compact remote source, are clearly seen in HXRs, while during the first spike quite weak, if any, HXR emission is observed at the location of the remote source. In microwaves, relatively compact source cospatial with the HXR double is seen during the first spike. The microwave sources elongates to the direction of the HXR remote source.

Figure 4. shows light curves of the HXR double sources and the remote source in HXT L, M1, M2 and H-bands. The flux of the double sources is given by the average over the region including these two sources. Microwave brightness variations in corresponding two regions are also plotted in figure 4.. From this figure, we find that during the second spike the HXR remote source shows two sub-spikes with a duration of $\approx$ 3 s, while the double sources show a single peak, which coincides with the peak of the first sub-spike of the remote source. The microwave brightness temperature and the HXT M1-band flux at the location of the HXR remote source show quite similar temporal variations. In Table 2., the HXT L, M1, M2 and H-band fluxes for the double sources and the remote source during the first and second spikes, and the flux ratios between the L and M1-bands, M1 and M2-bands, and M2 and H-bands are listed. At the second sub-spike, the HXR flux spectrum of the remote source is harder than that of the double source. This result is confirmed by a comparison of the HXT L, M1, M1 and H-band images at the second sub-spike shown figure 5.. This figure also shows that two sources in the HXR close-double source have different spectra; the southwest source has softer spectrum compared with the northeast source.

5. SUMMARY AND DISCUSSION

We present results of an analysis of 25 impulsive solar flares, which are systematically selected from the flares observed simultaneously with the Nobeyama Radioheliograph and the *Yohkoh* satellite. The results are summarized as follows; (1) for half of the analyzed 25 events two, at least, flaring loops are involved, (2) typical sizes of the two loops are different from each other (one is typically $\leq 20''$ and the other $30''$–$80''$), and (3) in hard X-rays, the smaller one of the two loops is preferentially bright. These results are consistent with those given in a previous paper (Nishio et al. 1997), where they used a subset of analyzed 25 events. The results strongly suggest that the interaction of the two loops plays a dominant role in releasing magnetic energy and producing energetic electrons.

From a detailed analysis of two out of the 25 events, we find a triple source structure: a close-double source corresponding to footpoints of the short loop and a remote source located at a footpoint of the long loop, both related with a single event. From the results that the peak of the first spike of the close-double sources proceeds to that of the remote source, and the remote source becomes prominent at later phase of the event, the particle acceleration site seems to be located near the small loop. On the other hand, the close-double and the remote

sources do not necessarily show same HXR flux spectra; the spectrum of remote source is harder than that of the close double sources at the intensity maximum of the remote source. Time of flight along the long loop is quite short comparing with the observed delay between the HXR close double and remote sources, ≈ 2 s, for the electrons with the energy of order of few 10 keV. Thus, to the events analyzed a simple loop-loop interaction mechanism, in which the small and large loops connect to each other and the electrons accelerated near the reconnection region directly precipitate to the footpoints, cannot be applied. Another mechanisms, such as trapping and diffusion of high energy electrons in the longer loop, must be taken in account. Further analysis and theoretical interpretation relating to the flare source evolution is required.

ACKNOWLEDGMENTS

The authors wish to express their deepest thanks to K. Fujiki and H. Koshiishi for their works to improve the image quality of the Nobeyama Radioheliograph, and J. Sato for his work to improve the image quality of the HXT. Further thanks are due to the staffs of the Nobeyama Radioheliograph and the Solar Flare Telescope at Mitaka, and to the *Yohkoh* team, especially to the SXT team, for their hard work in the construction and the operation of these instruments.

References

Aschwanden, M. J., Wills, M. J., Hudson, H. S., Kosugi, T., Schwartz, R. A. 1996a, ApJ 468, 398
Aschwanden, M. J., Kosugi, T., Hudson, H. S., Wills, M. J., Schwartz, R. A. 1996b, ApJ 470, 1198
Gopalswamy, N., Raulin, J-P., Kundu, M. R. , Nitta, N., Lemen, J. R., Herrmann, R., et al. 1995, ApJ 455, 715
Hanaoka, Y. 1996, Sol. Phys. 165, 275
Hanaoka, Y. 1997, Sol. Phys. 173, 319
Heyvaerts, J., Priest, E. R., Rust, D. M. 1977 ApJ 216, 123
Hoyng, P., Marsh, K. A., Zirin, H., Dennis, B. 1983 ApJ 268, 865
Kosugi, T., Makishima, K., Murakami, T., Sakao, T., Dotani, T., et al. 1991, Sol. Phys. 136, 17
Kawabata, K., Ogawa, H., Takakura, T. et al. 1982, Proc. Hinotori Symp., ed. Y. Tanaka, Tokyo, 168
Kundu, M. 1984, Adv. Space Res. 4, No 7, 157
Kundu, M., Nitta, N., White, S. M., Shibasaki, K., Enome, S., et al. 1995, ApJ 454, 522
Masuda, S., Kosugi, T., Hara, H., Tsuneta, S., Ogawara Y. 1994, Nature 371, 495
Nakajima, H., Dennis, B. R., Hoyng, P., Nelson, G., Kosugi, T., et al. 1985, ApJ 288, 806
Nakajima, H., Nishio, M., Enome, S., Shibasaki, K., Takano. T., et al. 1994, Proc. IEEE 82, 705
Nishio, M., Nakajima, H., Enome, S., Shibasaki, K., Takano. T., et al. 1994, Proc. Kofu Symp., ed. by S. Enome and T. Hirayama, NRO Rep. 360, 19
Nishio, M., Yaji, K., Kosugi, T., Nakajima, H. Sakurai, T. 1997, ApJ 489, 976
Nishio, M., Yaji, K., Kosugi, T., Nakajima, H. 1998, Adv. Space Res., submitted
Sato, J. 1997, Ph. D. Dissertation, The Graduated University for Advanced Studies
Shibata, K. 1998, Observational Plasma Astrophysics: Five Years of Yohkoh and Beyond, ed. Watanabe T., et al., Kluwer, 187
Takakura, T., Ohki, K., Tsuneta, S., Nitta, N. 1983, Sol. Phys. 86, 323
Takakura, T., Nishio, M., Nakajima, H., Enome, S., Shibasaki, K., et al. 1994, PASJ 46, 653
Tsuneta, S. 1996, ApJ 456, 840
Tsuneta, S., Acton, L., Bruner, M., et al. 1991, Sol. Phys. 136, 37
Tsuneta, S., Hara, H., Shimizu, T., Acton, L. W.. Strong, K. T., et al. 1992, PASJ 44, L63
Wang, H., Gary, D. E., Zirin, H., Schwartz, R. A., Sakao, T., et al., 1995, ApJ 453, 505
Wang, H., Gary, D. E., Zirin, H., Nitta, N., Schwartz, R. A., et al. 1996, ApJ 456, 403